

Comparisons of Ground Motions from Five Aftershocks of the 1999 Chi-Chi, Taiwan, Earthquake with Empirical Predictions Largely Based on Data from California

by Guo-Quan Wang, David M. Boore, Heiner Igel, and Xi-Yuan Zhou

Abstract The observed ground motions from five large aftershocks of the 1999 Chi-Chi, Taiwan, earthquake are compared with predictions from four equations based primarily on data from California. The four equations for active tectonic regions are those developed by Abrahamson and Silva (1997), Boore *et al.* (1997), Campbell (1997, 2001), and Sadigh *et al.* (1997). Comparisons are made for horizontal-component peak ground accelerations and 5%-damped pseudoacceleration response spectra at periods between 0.02 sec and 5 sec. The observed motions are in reasonable agreement with the predictions, particularly for distances from 10 to 30 km. This is in marked contrast to the motions from the Chi-Chi mainshock, which are much lower than the predicted motions for periods less than about 1 sec. The results indicate that the low motions in the mainshock are not due to unusual, localized absorption of seismic energy, because waves from the mainshock and the aftershocks generally traverse the same section of the crust and are recorded at the same stations. The aftershock motions at distances of 30–60 km are somewhat lower than the predictions (but not nearly by as small a factor as those for the mainshock), suggesting that the ground motion attenuates more rapidly in this region of Taiwan than it does in the areas we compare with it. We provide equations for the regional attenuation of response spectra, which show increasing decay of motion with distance for decreasing oscillator periods. This observational study also demonstrates that ground motions have large earthquake-location-dependent variability for a specific site. This variability reduces the accuracy with which an earthquake-specific prediction of site response can be predicted.

Online Material: PGAs and PSAs from the 1999 Chi-Chi earthquake and five aftershocks.

Introduction

The high-frequency ground motions from the 1999 Chi-Chi, Taiwan, mainshock (M 7.6) were found to be on average about 0.4 times the motions from empirical ground-motion prediction equations, based largely on data from California (e.g., Anderson *et al.*, 2000; Somerville, 2000; Boore, 2001b; Wang, 2001). Other recent earthquakes (e.g., 1999 Kocaeli earthquake, 1999 Hector Mine earthquake, and 2002 Denali earthquake) have also produced smaller-than-expected high-frequency motions, and various suggestions have been made as to why this is so (Anderson *et al.*, 2002; Somerville, 2003; Ellsworth *et al.*, 2004). It is not clear what to do with these data in deriving new ground-motion prediction equations. If the low motions are due to some unusual attenuation in the vicinity of the recordings, then it would not be proper to combine the data with those from other parts of

the world. On the other hand, if the low motions are due to some properties of the source that might also exist in the other parts of the world (such as if the rupture extends to the surface, as suggested by Somerville, 2000), then the derivation of new ground-motion prediction equations must account for this complication. In this article we study the ground motions from five aftershocks of the 1999 Chi-Chi, Taiwan, earthquake to see if those motions are also smaller than expected from equations based on ground motions elsewhere. We find that the aftershock motions are not as deficient at high frequencies as are the mainshock motions, particularly if an apparent difference in attenuation with distance is taken into account. Significant event-to-event variability occurs in the ground motions at a single station, however, but our overall conclusions seem to hold despite this variability.

Data: Sources and Processing

Of the five aftershocks used in this study, the moment magnitudes of four are near M 6.2, with one having a magnitude of M 5.8. Four of the aftershocks have a reverse-slip mechanism and one has a strike-slip mechanism. The source properties of the five aftershocks are given in Table 1, taken largely from the work of Chi and Dreger (2004), who inverted the strong-motion data for many of the source parameters. We compare the peak horizontal accelerations and the response spectra with those predicted from four commonly used empirical equations for active tectonic regions: Abrahamson and Silva (1997), Boore *et al.* (1997), Campbell (1997, 2000), and Sadigh *et al.* (1997), which are abbreviated as AS97, B97, C2000, and Sea97, respectively. (Campbell [1997] was updated recently by Campbell and Bozorgnia (2003), but the bulk of our work was completed before the update was available.) Figure 1 shows the location of the epicenters of the Chi-Chi mainshock and five aftershocks, and the 128 stations ($r_{rup} \leq 60$ km) used in computing the average ratios of response spectra, including 12 stations on *B* sites, 28 stations on *C* sites, and 88 stations on *D* sites. The site classes source from Lee *et al.* (2001a). The sparse station coverage in the central part of Taiwan is because it is occupied by the Central Mountain Ranges with peaks up to 4000 m.

The free-field acceleration data are from the Central Weather Bureau of Taiwan (CWB) Strong-Motion Data Series CD-002 (for aftershocks 1803, 0014, and 2352) and CD-003 (for aftershocks 1757 and 2146) distributed by Lee *et al.* (2001b, c). There are 249, 329, 300, 303, and 249 three-component records available for the five aftershocks 1803, 0014, 2352, 1757, and 2146 from CD-002 and CD-003. (The five aftershocks were named according to their origin times; see Table 1.) The data for the two horizontal components were used in this study. In previous studies (Boore, 1999, 2001a; Wang, 2001; Wang *et al.*, 2001, 2002, 2003), we found that almost all recordings of the mainshock were plagued by random baseline offsets. We have found the same thing for the aftershock recordings. An important conclusion from our previous work is that for earthquake-engineering

purposes the response spectra for periods less than about 20 sec are usually unaffected by the baseline corrections (Boore, 1999, 2001a; Wang, 2001). In the present study we need only response spectra between 0.02 and 5 sec. (This period range includes the ranges used by the various empirical ground-motion prediction equations.) Therefore we simply applied a fourth-order causal Butterworth low-cut filter with corner frequency of 0.02 Hz to the records, after removing the mean of the entire record from the whole record. For comparison with the prediction equations, the geometric

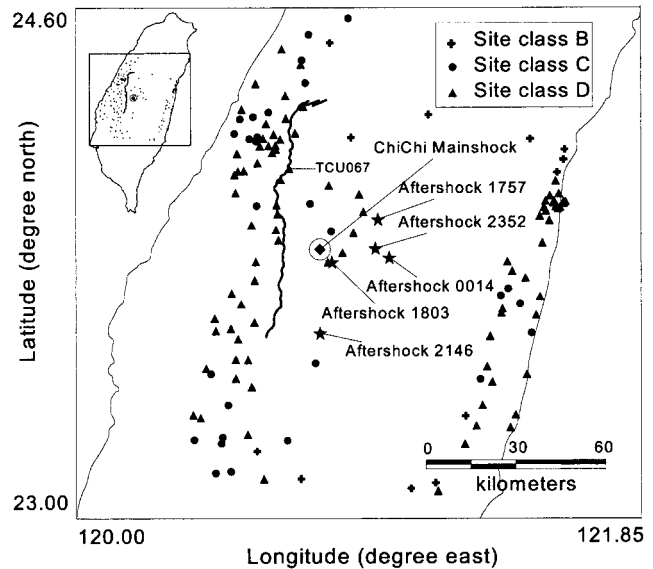


Figure 1. Map showing the epicenters of the five aftershocks and the locations of the 128 stations ($r_{seis} \leq 60$ km) used in studying ratios of observed-to-predicted response spectra in this study. The different symbols represent different stations located on different site classes, including 12 stations on *B* sites, 28 stations on *C* sites, and 88 stations on *D* sites. The site classes are from Lee *et al.* (2001a). The large circle indicates the epicenter of the 1999 Chi-Chi mainshock, and the curve on its left side represents the Chelungpu fault, which was the causative fault of the Chi-Chi mainshock.

Table 1

Main Source Parameters of the Five Aftershocks of the 1999 Chi-Chi, Taiwan, Earthquake Studied in This Article*

| Event [†] | Origin time (UT, mm/dd/yy, h:m:s) | Epicenter (degree) | | Depth (km) | M_L | M_w | Strike (degree) | Dip (degree) | Rake (degree) | Asperity Area (km ²) | Rupture Size (L × W) (km ²) |
|--------------------|--------------------------------------|--------------------|-----------------|---------------|-------|-------|--------------------|-----------------|------------------|-------------------------------------|--|
| | | Longitude (E) | Latitude (N) | | | | | | | | |
| 0014 | 09/22/99, 00:14:40.770 | 121.08 | 23.81 | 10 | 6.8 | 6.2 | 165 | 70 | 100 | 120 | 15 × 8 = 120 |
| 1803 | 09/20/99, 18:03:41.160 | 120.86 | 23.81 | 8 | 6.6 | 6.2 | 0 | 10 | 80 | 100 | 15 × 8 = 120 |
| 2352 | 09/25/99, 23:52:49.509 | 121.01 | 23.87 | 16 | 6.8 | 6.3 | 5.0 | 30 | 100 | 132 | 17 × 9 = 153 |
| 1757 | 09/20/99, 17:57:15.310 | 121.01 | 23.94 | 8 | 6.4 | 5.8 | 200 | 41 | 78 | 48 | 9 × 6 = 54 |
| 2146 | 09/20/99, 21:46:37.490 | 120.82 | 23.60 | 18 | 6.6 | 6.2 | 330 | 89 | 15 | 125 | 18 × 8 = 414 |

*The parameters of the epicenter, depth, M_w , strike, dip, rake and asperity area are from Chi and Dreger (2004). Origin time and M_L are from Lee *et al.* (2001b,c). The rupture sizes of the five events are estimated according to the empirical relationship between earthquake magnitude and fault parameters developed by Wells and Coppersmith (1994).

[†]The five aftershocks are named according to their origin times.

mean of the peak horizontal accelerations (PHAs) and the 5%-damped pseudoacceleration (PSA) response spectra were computed.

Prediction of Motions

Ground-motion prediction equations, which estimate peak ground motions or response spectral ordinates as a function of earthquake magnitude, distance, and other parameters, are a critical component of seismic hazard analysis. In this article we compare the ground motions of the five large Chi-Chi, Taiwan, aftershocks with four commonly used prediction equations based in large part on data from California. As both areas are active tectonically, the hope is that the California data would be similar to those from Taiwan. These equations have as predictor variables the magnitude of the earthquake, the distance to the station, and some measures of the type of site and the type of faulting. All of the equations use moment magnitude as the measure of earthquake size, but the other variables are not the same for each equation, as discussed now.

Three measures of the source-to-site distance are used in the four prediction equations. AS97 and Sea97 use the closest distance to the rupture plane (r_{rup}); BJF97 uses the closest horizontal distance from the station to the projection of the rupture surface onto Earth's surface (r_{jb}); C2000 uses the shortest distance between the recording site and the presumed zone of seismogenic rupture on the fault (r_{seis}), which is same as r_{rup} except that the rupture surface is assumed to extend no shallower than the seismogenic depth of 3.0 km. The size and location of the fault-rupture surface for the five aftershocks are not well known. Therefore, we estimated the rupture size from the empirical relationships for fault length L and area A given by Wells and Coppersmith (1994). For the reverse-slip faults we used:

$$\log(L) = -2.42 + 0.58M \quad (1)$$

and

$$\log(A) = -3.99 + 0.98M. \quad (2)$$

For the strike-slip fault we used

$$\log(L) = -2.57 + 0.62M \quad (3)$$

and

$$\log(A) = -3.42 + 0.90M \quad (4)$$

We obtained the fault width W from L and A . From these equations we estimated the rupture sizes given in Table 1; the areas compare relatively well with the asperity areas obtained by Chi and Dreger (2004) from inverting strong-motion data. (The asperity areas are also given in Table 1.) We center the estimated rupture surface on the hypocenter

and use this in the calculation of distances. Because the rupture surfaces of the five events are not shallower than 3.0 km, r_{rup} and r_{seis} are same for all stations of the five events.

The specification of site conditions in the four empirical ground-motion prediction equations ranges from generic rock and soil in AS97 and Sea97 to the use of average shear velocity in the upper 30 m in BJF97. Following the recommendations in Campbell (2000), we set the variables as follows: for generic rock motions, $S_{\text{SR}} = 1$, $S_{\text{HR}} = 0$, and $D = 1$ km; for generic soil motions, $S_{\text{SR}} = 0$, $S_{\text{HR}} = 0$, and $D = 5$ km, where S_{SR} and S_{HR} are variables indicating soft rock and hard rock sites, respectively, and D is the depth to basement rock. For use in each set of equations, we use the assignments of Lee *et al.* (2001a) for the seismic stations that recorded the Chi-Chi mainshock and aftershock ground motions. The scheme of Lee *et al.* is similar to the 1997 NEHRP (National Earthquake Hazards Reduction Program, Building Seismic Safety Council [BSSC], 1998) classification, which assigns sites to classes *A*, *B*, *C*, *D*, or *E* according to $\bar{V}_s(30)$ (Lee *et al.* estimated $\bar{V}_s(30)$ from geological descriptions). We reclassified the stations into rock and soil classes according to the following scheme: class *B* and *D* sites are taken as rock and soil, respectively; and the 28 class *C* sites used in the analysis are classified as soil if located on the northwest side (see Fig. 1) of the Chelungpu fault (12 sites) and rock otherwise (16 sites). It is reasonable to expect that geologic materials under the *C* sites for the eastern and western stations are different. The western stations are on the Coastal Plain with thicker and finer-grained soils, whereas the eastern stations are at the foot of young and steep mountains with thinner soils. Note that no records from *E* sites were included in the databases used to develop the four prediction equations, and therefore no *E* sites are used in this study.

The effect of source mechanism is captured by a style-of-faulting variable (F) according to the type of faulting (usually in a binary manner). C2000 uses a constant factor that applies to all magnitude, distance, and oscillator periods, with $F = 0$ for strike-slip faulting, $F = 1$ for reverse-slip faulting, thrust, reverse-oblique, and thrust-oblique faulting (rake angles greater than 22.5°), and $F = 0.5$ for faulting whose mechanism is unknown. Sea97 distinguishes between strike-slip and reverse-faulting earthquakes (rake angles greater than 45°). BJF97 uses a period-dependent style-of-faulting factor for strike-slip and reverse-slip events (rake angles greater than 30°), and AS97 uses a magnitude- and period-dependent style-of-faulting factor (the rake angles for the various fault types are not specified in their article). The rake angles of the five aftershocks studied in this paper are given in Table 1. It can be seen that all events except the event 2146 are classified as reverse-slip earthquakes.

Comparisons of Observed and Earthquake-Site-Specific Predicted Ground Motions

In this section, we compare the observed motions with earthquake- and site-specific predictions. The horizontal

peak ground acceleration (PHA) and 5%-damped response spectra at 0.2 sec and 2.0 sec (PSA-0.2, PSA-2.0) are studied, which represent the ground motion at short, short-middle, and middle-long period ranges. The 0.2-sec oscillator period generally corresponds to the period range of peak acceleration response for the five events. The predictions of Boore *et al.* (1997) use a quantitative measure for the site classification based on the average shear-wave velocity in the upper 30 m, which is consistent with the site classification scheme for Taiwan's seismic stations given by Lee *et al.* (2001a). Therefore, we first do the comparisons of observations and predictions of Boore *et al.* (1997) at sites *B*, *C*, and *D*. We then do the comparisons for the other equations at soil and rock sites.

Figure 2 illustrates the comparisons of the observed PHAs and PSAs for 0.2- and 2.0-sec oscillator periods caused by the three **M** 6.2–6.3 reverse-slip earthquakes with the predictions from Boore *et al.* (1997). The motions for the mainshock are shown by the gray symbols. The first column shows the comparisons for the PHAs, and the second and the third columns are the comparisons for the 5%-damped pseudoacceleration response spectra for 0.2- and 2.0-sec oscillator periods, respectively. From the first row to the third row are the comparisons for site classes *B*, *C*, and *D*, respectively. Geometric means of the velocity values at the boundaries of the site classes are used in the equations of Boore *et al.* (1997) for estimating ground motion for the NEHRP site classes *B*, *C*, and *D*; these values are 1070 m/sec, 520 m/sec and 250 m/sec, respectively (the important findings of our study do not depend on the value of the specific velocities used to represent each site class). The predicted motions are shown only to 80 km in Figure 2, which is the maximum distance to be used in the Boore *et al.* (1997) equations. The results in Figure 2 indicate considerable scatter from one event to another, with the motions from EQ1803 being generally much smaller than those from the other two events. Except for that event, the motions compare reasonably well with the motions predicted from equations based largely on data from California; this is a distinctly different conclusion than for the mainshock motions, which are much lower than California motions for periods shorter than about 1 sec (Boore, 2001b; Wang, 2001). It also seems that the observed aftershock motions decay with distance more rapidly than the predictions of the BJF97. This is particularly true for PHA and PSA-0.2 sec at *D* sites. Later we derive attenuation factors for the Taiwan area. The mainshock motions for PHA and the 0.2-sec oscillator are similar to the aftershock motions (with the exception of aftershock EQ1803) and are greater than the aftershock motions for the 2.0-sec oscillator. For the two shorter-period measures of ground motion, the mainshock motions are similar to the Boore *et al.* (1997) predictions for M_w 6.2, emphasizing the anomalously low values for the mainshock documented by others. There is a wider separation between the mainshock and the aftershock motions for the 2.0-sec period oscillator,

as expected for motions from earthquakes of such different sizes.

To emphasize the difference between observed and predicted ground motions, from here on we discuss only the ratio of observed-to-predicted response spectrum (recalling that the observed motions are the geometric mean of the two horizontal component motions). The results for the individual earthquakes are shown in Figure 3, separated into rock and soil sites. The ratios are computed for the four ground-motion prediction equations. Stations were excluded from the analysis if $r_{\text{seis}} > 60$ km, which is the distance criteria used by Campbell (1997) in his prediction equations. This is the smallest upper-limit distance of the four empirical equations. The lines represent the uncertainties of a single observation, as given by the standard deviation of the predicted motion (the lines are given by $e^{\pm\sigma \ln Y}$); if the observations were consistent with those used to derive the prediction equations, we would expect 68% of the observations to fall within the two lines. Figure 3 shows that most of the ratios of the five events fall within the range of uncertainty in the prediction of a single motion, although there are clearly systematic exceptions to this for individual events. There is considerable earthquake-to-earthquake variation, and this variation is larger than the variation among the prediction equations. The next section looks at the means of ratios within a certain distance range as a different way of studying the relative differences between observed and predicted ground motions.

Average Ratios in Distance Bins

As illustrated in Figures 2 and 3, the ratios of observed-to-predicted motions are widely scattered. It seems that PHAs and PSAs for 0.2 sec are somewhat smaller on average than the predictions, especially for distances greater than 30 km, suggesting a different rate of distance decay than for the California data. The observed and predicted PSAs seem to be in better agreement for the 2.0-sec oscillator. To study the comparison for a more complete set of oscillator periods, we now look at the geometric mean of ratios falling within a distance bin as a function of oscillator period. Based on Figures 1, 2, 3, and following Boore (2001b), we use distance bins of $10 < r_{\text{rup}} \leq 30$ km and $30 < r_{\text{rup}} \leq 60$ km. The number of the data in different distance bins is listed in the Table 2. Altogether, 316 horizontal-component records at soil sites and 56 horizontal-component records at rock sites from the five events are used in this analysis. We do not show ratios for rock sites in the distance range $10 < r_{\text{rup}} \leq 30$ km because there are only seven records in that distance bin, a number too small for statistical analysis.

Figure 4 illustrates the means of the ratios of observed-to-predicted motions for each earthquake separately. Note that the mean ratios for PHAs are plotted at $T = 0.015$ sec for graphical convenience. (We are not claiming that the PSA reaches the PGA value at that period.) For the aftershock 0014 there are no records in the first distance bin. The four

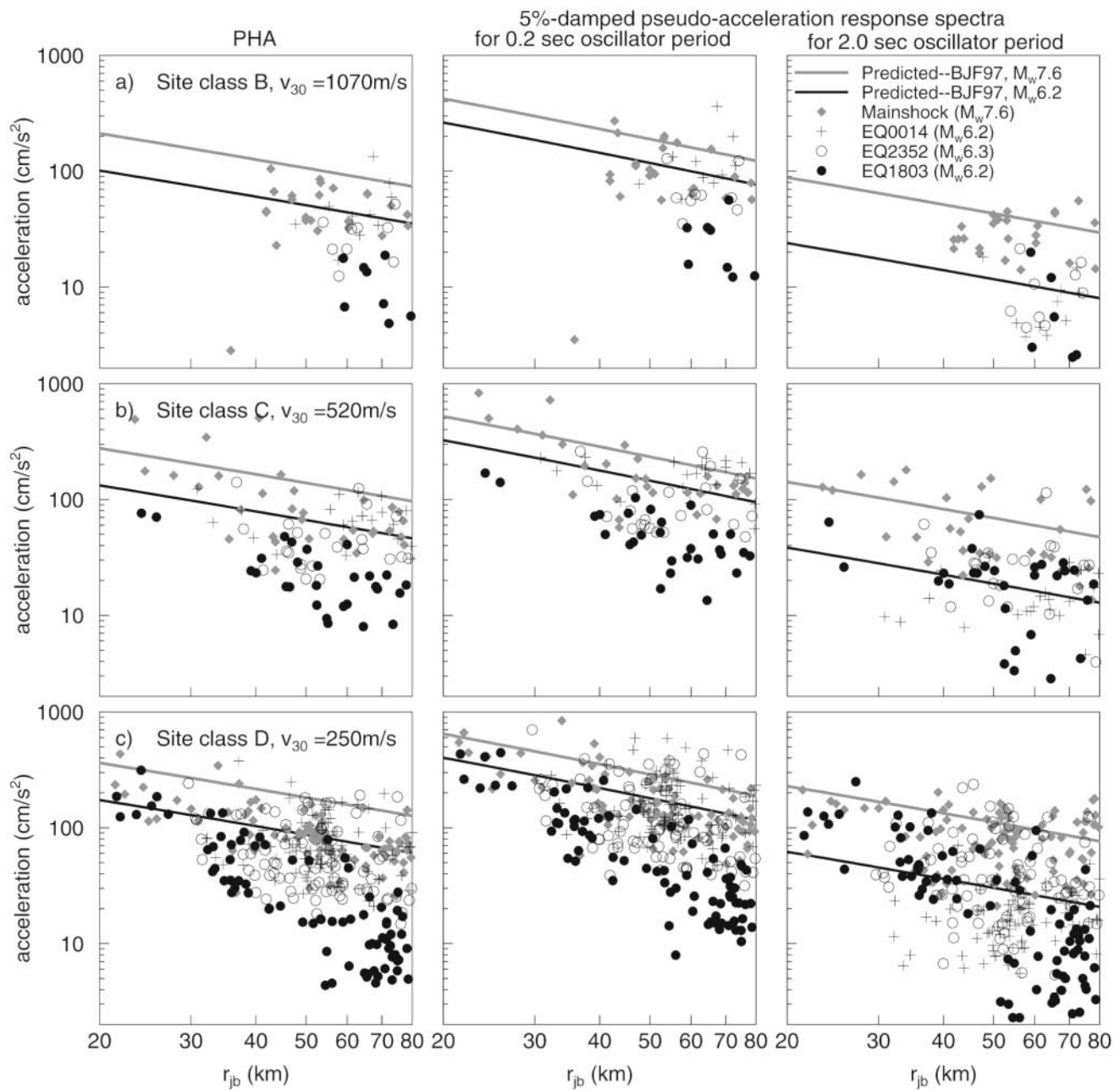


Figure 2. Comparisons of observed horizontal-component ground motions on different sites caused by the three reverse-slip aftershocks with magnitudes near M 6.2 (EQ0014, M 6.2; EQ1803, M 6.2; and EQ2352, M 6.3) with the predictions from the Boore *et al.* (1997) equations. The gray symbols represent the mainshock motions. The lines illustrate the predictions from the Boore *et al.* (1997) equations. The first column illustrates the comparisons for the horizontal-component peak ground accelerations (PHAs) on site class *B* (a, the first row), site class *C* (b, the second row), and site class *D* (c, the third row). The second and the third columns illustrate the comparisons for the 5%-damped pseudoacceleration response spectra (PSAs) for 0.2-sec and 2.0-sec oscillator periods, respectively. The observed horizontal ground motions are the geometric means of the values recorded by the two horizontal components (north-south and east-west) of the accelerographs.

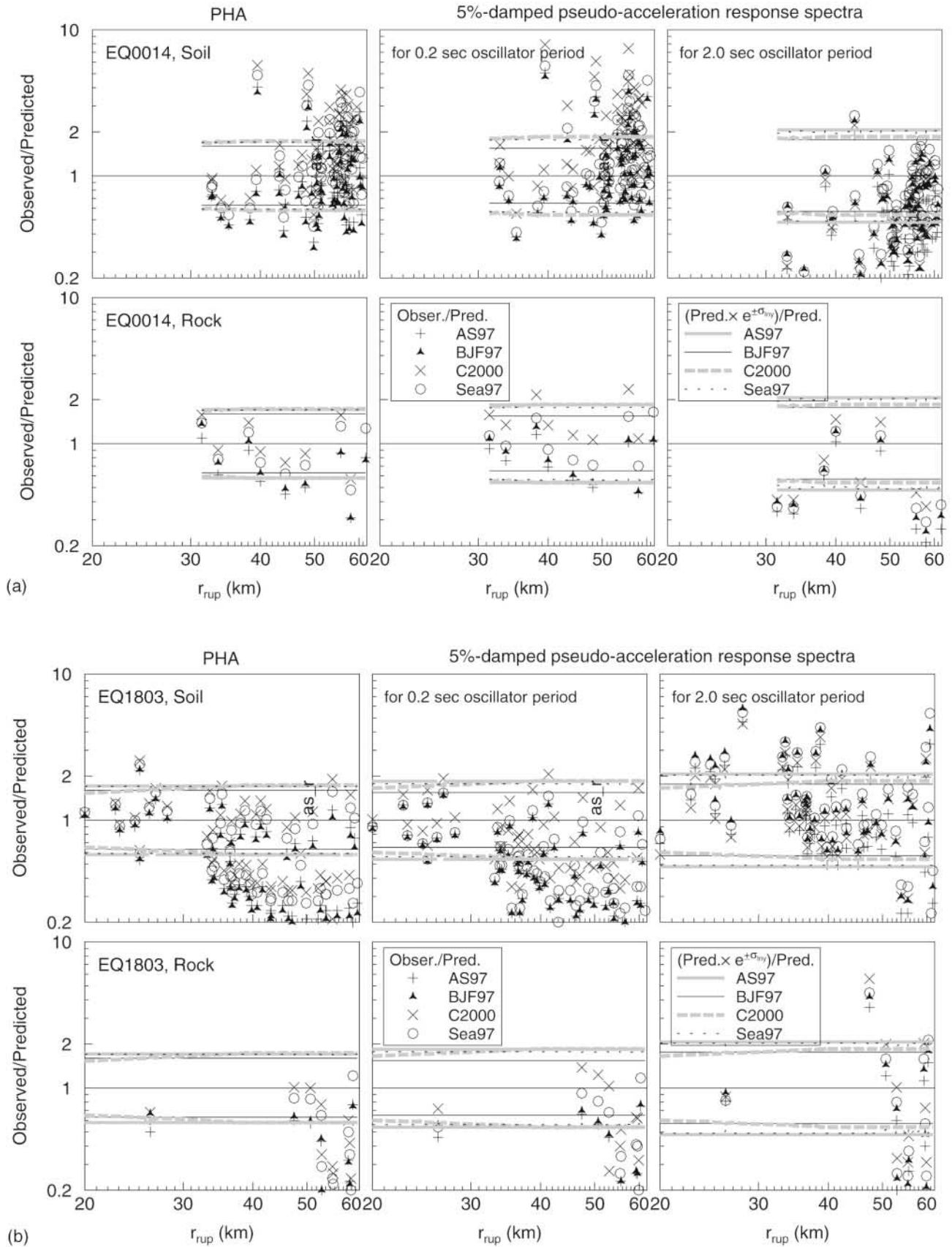
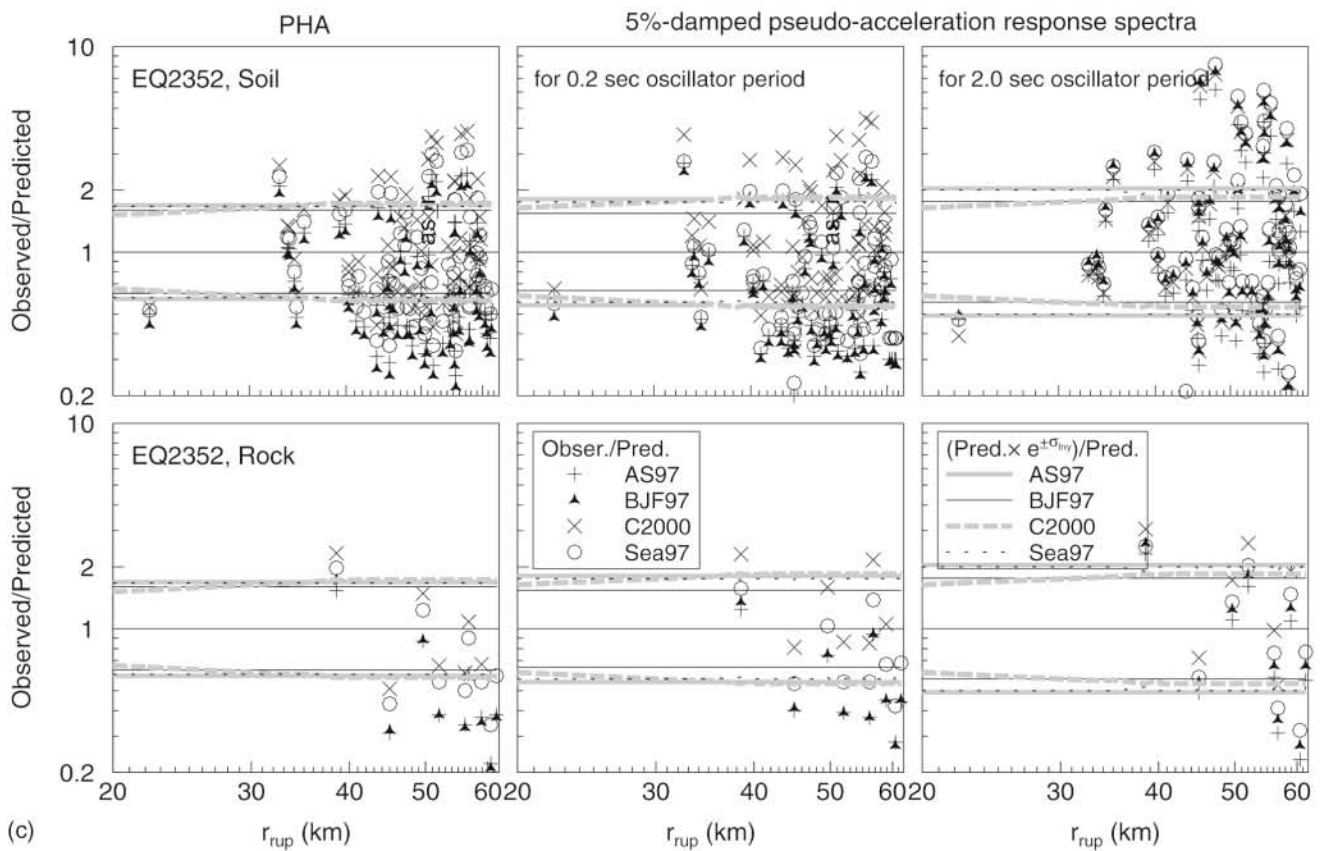
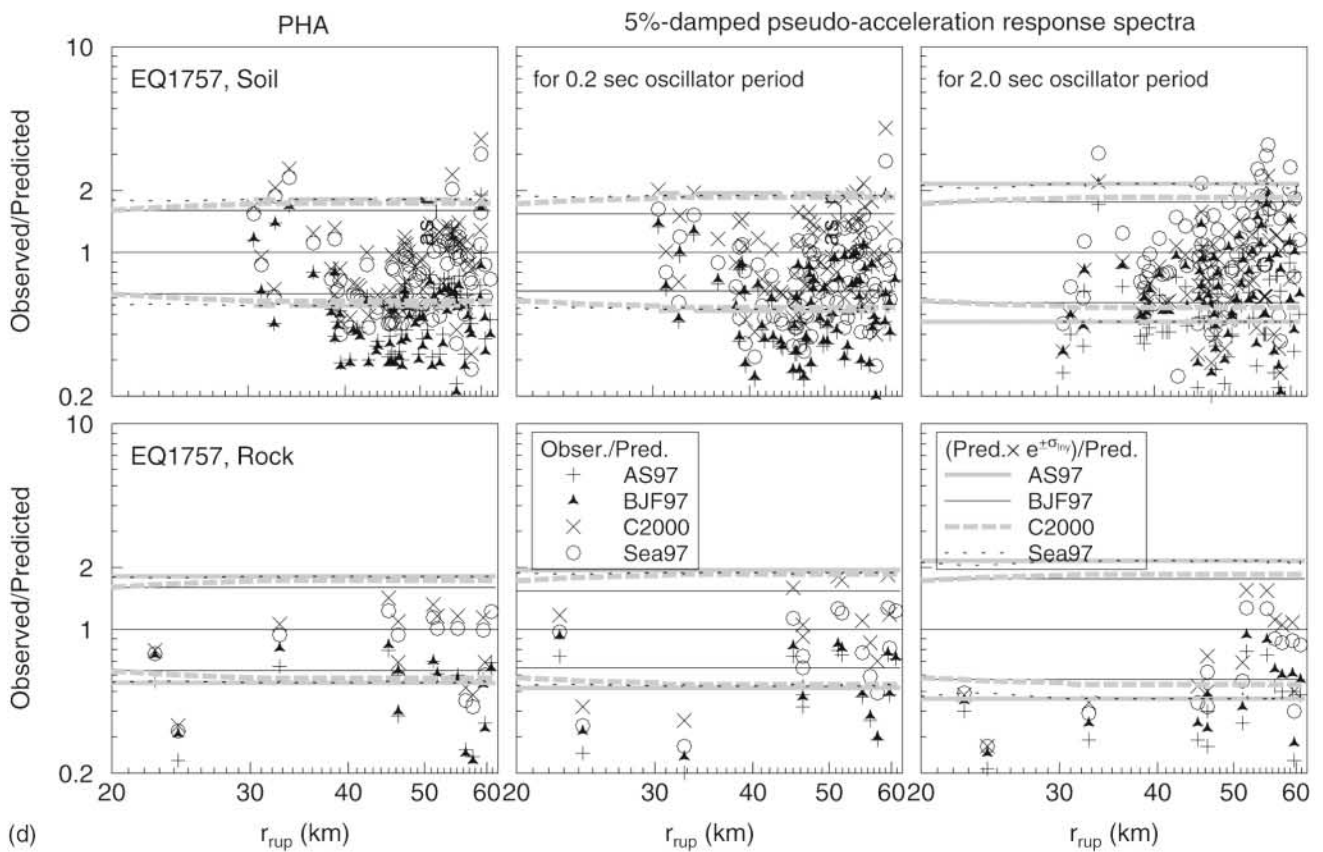


Figure 3. (Continued on following pages.)



(c)



(d)

Figure 3. (Caption on next page.)

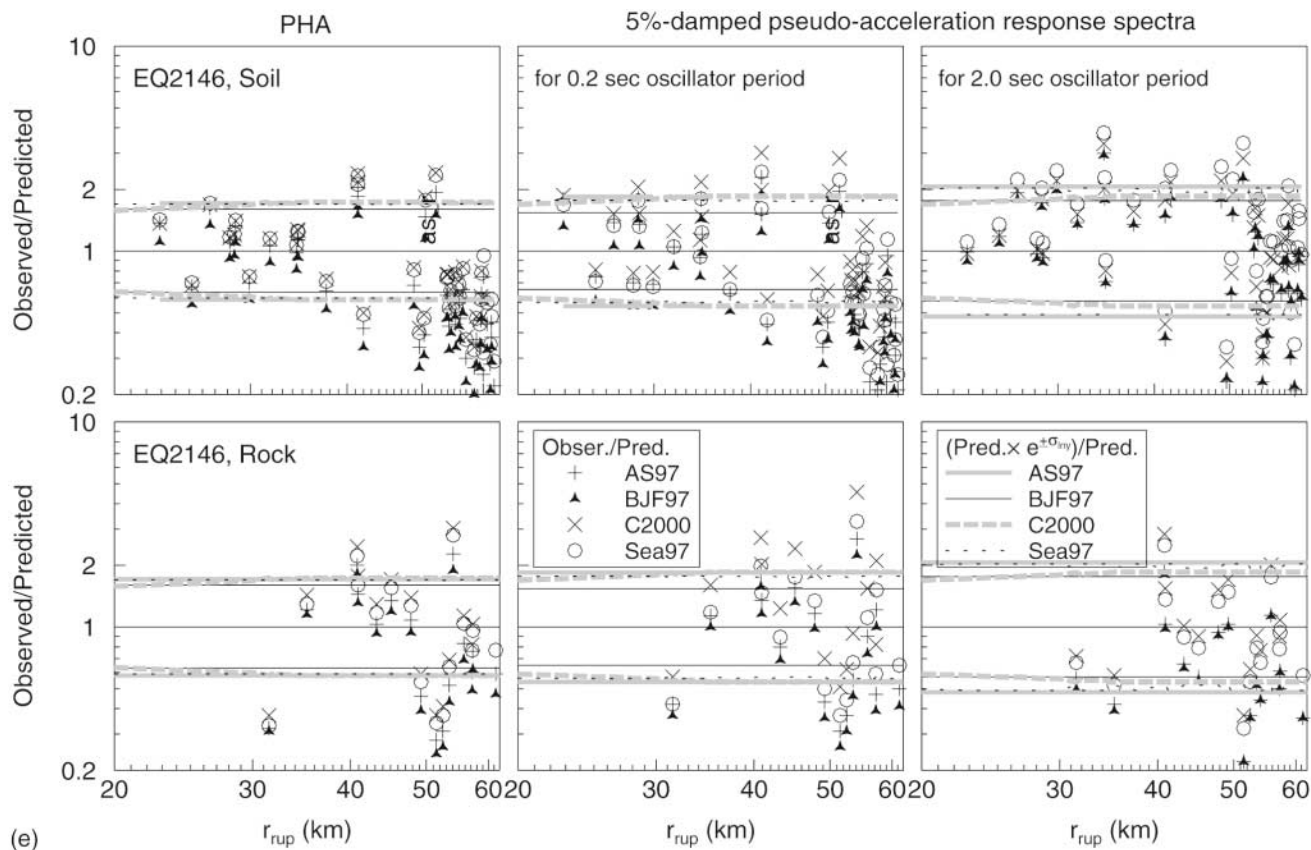


Figure 3. (Continued) The ratios of the observed PHAs (the first column) and 5%-damped pseudoacceleration response spectra for 0.2 sec (the second column) and 2.0 sec (the third column) oscillator periods to predictions of the four equations Abrahamson and Silva (1997), Boore *et al.* (1997), Campbell (1997, 2000), and Sadigh *et al.* (1997). Subfigures a, b, c, d, and e illustrate the ratios for aftershocks 0014, 1803, 2352, 1757 and 2146, respectively. The soil sites include *D* sites and 12 *C* sites located at the northwest side of the Chelungpu fault; the rock sites include all *B* sites and other *C* sites. Different symbols represent the ratios corresponding to different predictions. The lines represent the uncertainties in the predictions of ground motion from a single station, as given by lines plotted at $e^{\pm \ln Y}$.

Table 2

Numbers of Samples ($r_{\text{seis}} \leq 60$ km) in Different Distance Bins of Figures 4 and 5

| Aftershock | Number of Records on the Soil Site | | Number of Records on the Rock Site | | Total |
|---------------------------|------------------------------------|----------|------------------------------------|----------|-------|
| | 0–30 km | 30–60 km | 0–30 km | 30–60 km | |
| | | | (not analyzed) | | |
| 0014 | 0 | 62 | 0 | 9 | 71 |
| 1803 | 16 | 49 | 3 | 10 | 78 |
| 2352 | 4 | 69 | 0 | 9 | 82 |
| 1757 | 4 | 71 | 3 | 12 | 90 |
| 2146 | 7 | 34 | 1 | 16 | 58 |
| Total of five aftershocks | 31 | 285 | 7 | 56 | 379 |
| Chi-Chi main shock | 64 | 58 | 9 | 36 | 167 |

prediction equations are indicated by the different symbols, and to help judge the size of the observed-to-predicted ratio, horizontal lines are plotted at ratios of 0.5, 1.0, and 2.0. (The prediction uncertainties shown in Fig. 3 are not shown here because those uncertainties are for the predictions of individual points rather than the mean of a number of points, which would reduce the uncertainty by approximately the square root of the number of points within a distance bin.) Although differences exist, the overall trends of the ratios are similar for the various prediction equations. There are significant trends with oscillator period, and a large earthquake-to-earthquake variability in the ratios, making accurate predictions of earthquake-specific ground motions difficult.

To see better the overall comparison of observations and predictions, we average the ratios for each earthquake in each distance bin. The results are shown in Figure 5. In

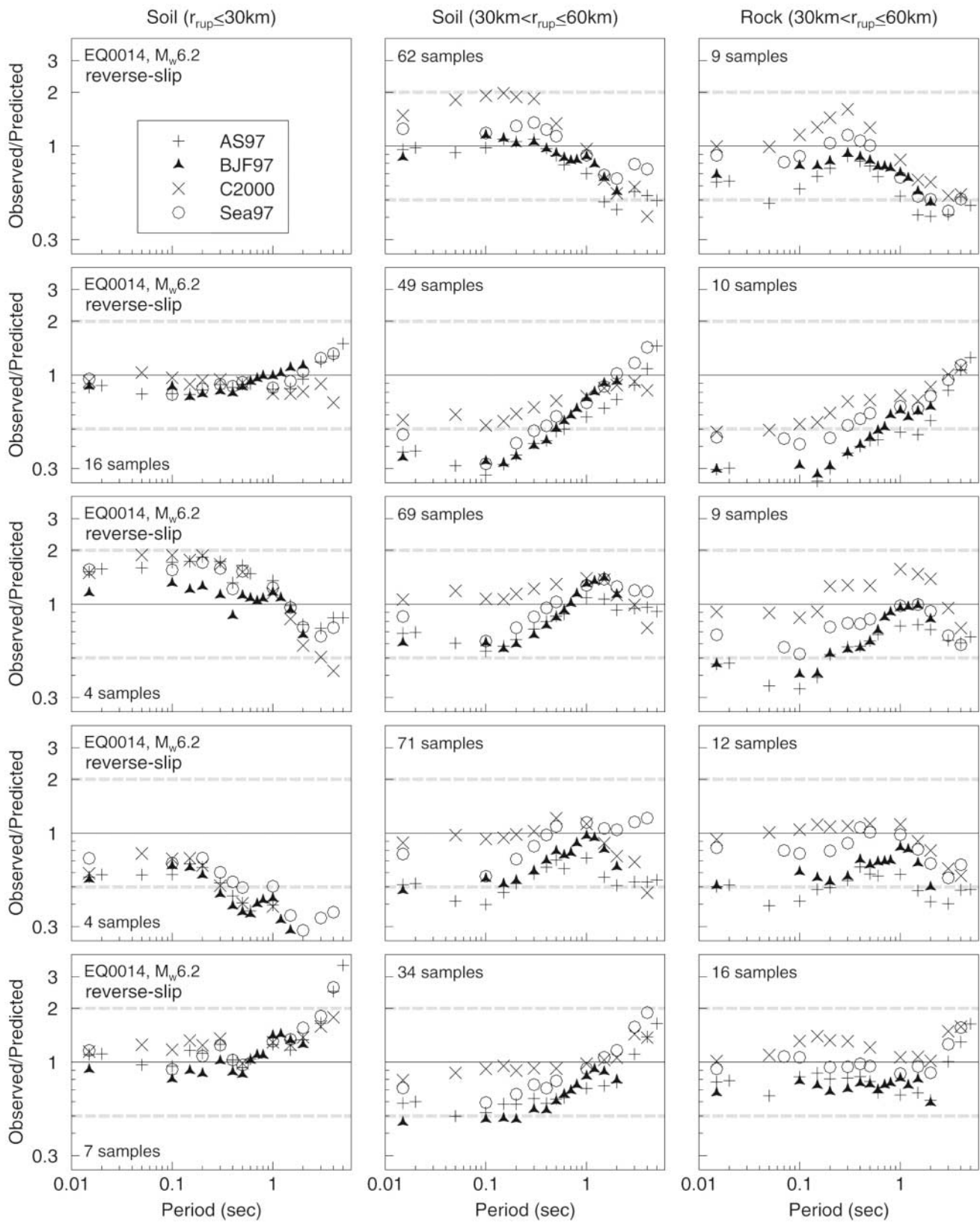


Figure 4. Geometric mean ratios of observed response spectra to the four predictions plotted against oscillator period for two distance groups (10–30 km and 30–60 km) for soil sites and one distance group (30–60 km) for rock sites. From the first row to the fifth row are the mean ratios for the aftershocks 0014, 1803, 2352, 1757, and 2146, respectively. Different symbols represent the ratios corresponding to different predictions. The ratios for PHA are plotted at $T = 0.015$ sec. The lines represent factors of 0.5, 1.0, and 2.0 and are intended to help in assessing the size of the ratio compared with unity (a perfect match).

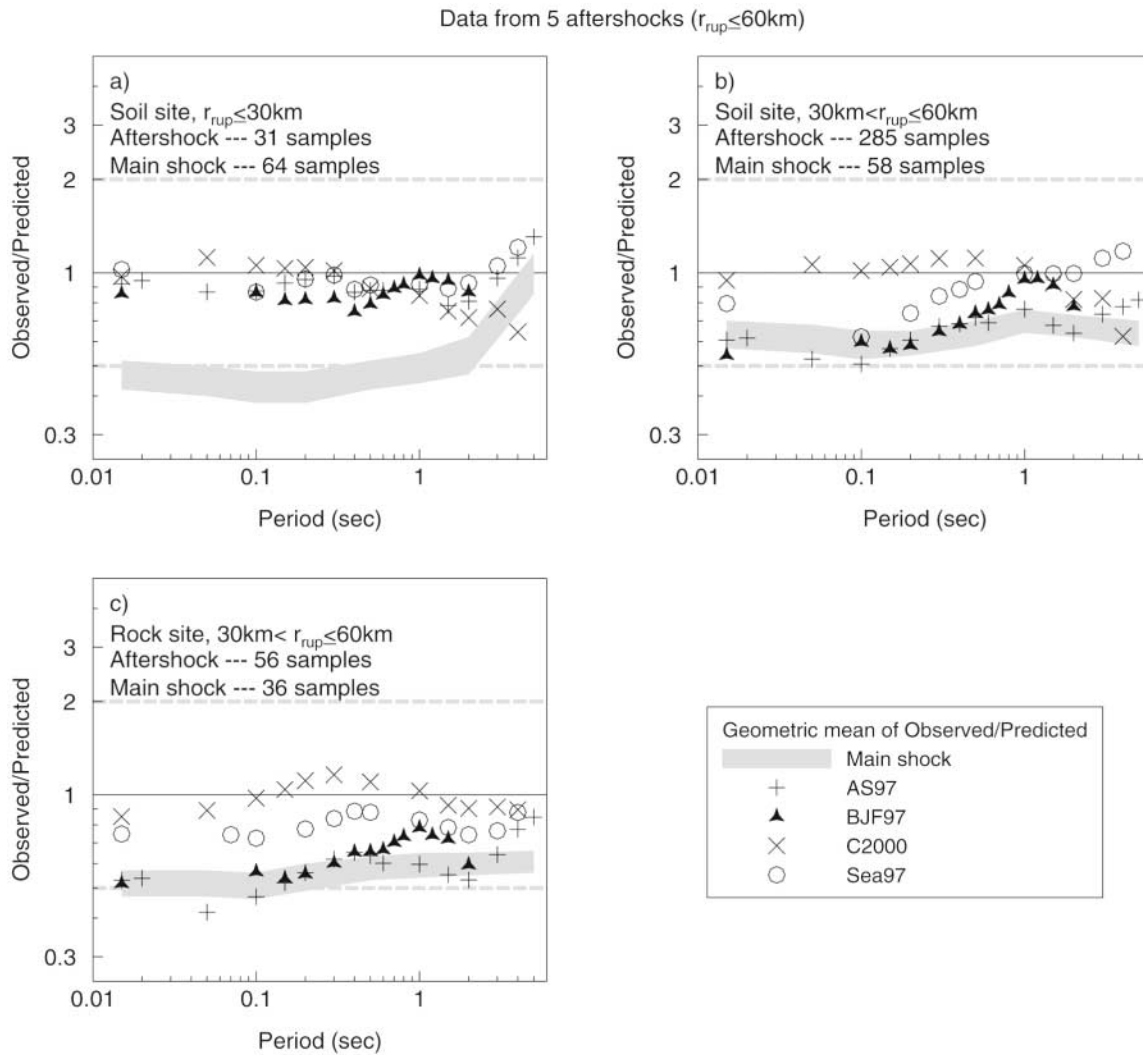


Figure 5. Same as Figure 4, but the geometric means of the records for all five events in the same distance bin are plotted. The gray bands indicate the average range of ratios for the 1999 Chi-Chi mainshock motions to predictions from the same four ground-motion prediction equations.

addition, we indicate by the gray bands the ratios for the mainshock, as taken from the work of Boore (2001b), modified to account for the rock and soil classifications for each site (information not available when Boore [2001b] was published). The numbers of mainshock recordings used in this section are listed in Table 2. The gray bands indicate the range for the various prediction equations. We now see that the ratios for the aftershocks are systematically larger than those for the mainshock for almost all periods from 0.02 sec to 5 sec. It does not seem to be much different in the observed-to-predicted comparisons between rock and soil sites, and the ratio is near unity for the 10- to 30-km distance bin and less than unity for the 30- to 60-km bin, suggesting that the motions are decaying more rapidly with distance than those from California earthquakes.

Earthquake-to-Earthquake Variation: An Example

The comparisons illustrated in Figures 2, 3, and 4 indicate considerable difference in ground motion among the five aftershocks. To better understand the earthquake-to-earthquake variation and the difference between observations and earthquake-site-specific predictions, we analyze records from a single station (TCU067) located very close to the rupture area of the Chelungpu fault, the causative fault of the Chi-Chi mainshock. The location of the station is marked on Figure 1. Distance from the station to the source of the five events is listed in Table 3.

Figure 6 illustrates the three-component acceleration, velocity, and displacement time series obtained from the station TCU067 triggered by the five events. The station-to-

Table 3
Main Parameters of the Records from Station TCU067 Caused by the Five Aftershocks*

| Earthquake | M_w | Slip | r_{jb} (km) | r_{rup} (km) | r_{sets} (km) | PGA (cm/sec ²) | | | PGV (cm/sec) | | | Duration (sec) [†] | | |
|------------|-------|--------------|------------------|-------------------|--------------------|----------------------------|-------|-------|--------------|------|------|-----------------------------|------|------|
| | | | | | | UP | NS | EW | UP | NS | EW | UP | NS | EW |
| EQ0014 | 6.2 | Reverse-slip | 41 | 43 | 43 | 56.0 | 97.9 | 93.1 | 2.7 | 5.2 | 7.0 | 0.02 | 3.35 | 3.45 |
| EQ1803 | 6.2 | Reverse-slip | 26 | 27 | 27 | 65.7 | 206.5 | 165.6 | 6.2 | 10.9 | 10.3 | 0.02 | 5.5 | 5.8 |
| EQ2352 | 6.3 | Reverse-slip | 32 | 35 | 35 | 29.0 | 47.8 | 58.9 | 5.0 | 6.7 | 9.0 | 0 | 0 | 1.15 |
| EQ1757 | 5.8 | Reverse-slip | 31 | 33 | 33 | 78.4 | 97.0 | 173.0 | 2.2 | 8.1 | 11.6 | 0.40 | 0.88 | 1.48 |
| EQ2146 | 6.2 | Strike-slip | 48 | 50 | 50 | 16.1 | 20.0 | 22.3 | 2.6 | 3.3 | 4.0 | 0 | 0 | 0 |

*Station TCU067 locates at north latitude 24.0912 degree and east longitude 120.720, with an elevation of 73 m. The local site was categorized as the class *D* by Lee *et al.* (2001a). The accelerograph installed on the TCU067 station is the A900 model produced by Geotech.

[†]Duration is a bracketed duration with a threshold of 50 cm/sec².

source distances are marked in the first column of Figure 6a. The differences in waveforms of different events are obvious on the accelerograms but are most dramatic in the displacement time series. The velocities and displacements are obtained by single and double integrations of acceleration time series corrected by first removing the mean of entire record from the whole record, and second by filtering the record with a causal, fourth-order low-cut Butterworth filter with a corner frequency of 0.02 Hz. The PGAs and PGVs of these records are listed in Table 3.

Figure 7 shows the observed response spectra of the two horizontal components from the station TCU067 triggered by the four reverse-slip events (EQ0014, 1803, 2352, and 1757) and the earthquake-site-specific predictions. One of the most interesting features of this figure is the good agreement between observed and predicted motions at longer periods (e.g., >0.5 sec). The agreement is worse at shorter periods, with the observed spectra higher or lower than the predicted spectra. The motions for event 2146 are particularly anomalous, but the earthquake-to-station distance for this station is greater than that for the other earthquakes. As noted before, there is a suggestion that the ground motions attenuate more rapidly with distance than do those from California earthquakes. To take this into account in making the comparisons of motions at station TCU067, we developed a regional attenuation function using Joyner and Boore's maxlik program (Joyner and Boore, 1993) based on the data at the *D* sites of the four reverse-slip events. We fit the following equation to the 5%-damped pseudovelocity response spectra, computed by multiplying the relative displacement response by the factor $2\pi/T$, where T is the undamped natural period of the oscillator:

$$\log Y = a_1 + a_2 (M - 6) + a_3 \log \sqrt{r_{jb}^2 + h^2}, \quad (5)$$

where the distance term assumes that all the attenuation is accounted for by geometric spreading, which is a reasonable assumption when data for only a limited distance range are available, and the value of h was varied from 4.5 to 7.5 km. The choice of h made little difference in the results. The coefficients for $h = 5.5$ are given in Table 4. Y is the pseudovelocity response in centimeters per second. Because three

of the four earthquakes used in the analysis had a magnitude near M 6.2 and the other had a magnitude of M 5.8, little confidence should be placed in the magnitude coefficient (a_2) in Table 4; the distance term, however, should be better determined and shows an almost uniform tendency for less rapid decay as period increases. For comparison, Table 4 also includes the coefficient (b_5) of the distance term in the BJF97 equations.

Figure 8 compares the 5%-damped pseudovelocity response spectra at the station TCU067 from the four reverse-slip events with and without correction for magnitude and distance dependence. The corrections were made from the magnitude (M) and distance (r_{jb}) of the observation to a magnitude and distance of 6.2 and 26 km, respectively, using the following equation:

$$\begin{aligned} \log Y_{\text{cor}}(6.2, 26) &= \log Y_{\text{obs}}(M, r_{jb}) \\ &+ \log Y_{\text{pred}}(6.2, 26) - \log Y_{\text{pred}}(M, r_{jb}) \end{aligned}$$

where Y_{obs} and Y_{pred} are the response spectra observed from the data and predicted from equation (5) and Table 4. The correction for differences in distance improves the comparison at the longer periods, but the large variability at most periods remains. It is not surprising that the distance correction cannot remove the variability, given that the uncorrected motions at 0.1 sec differ by up to a factor of 6, although the distance spread is only a factor of 1.6. No reasonable distance correction can account for a factor of 6 for a range of distance varying by only a factor of 1.6.

Conclusions

Observed peaks motions from five aftershocks of the 1999 Chi-Chi, Taiwan, mainshock agree reasonably well with the motions predicted from equations largely based on ground motions from California, particularly at distances from 10 to 30 km and for periods ranging from less than 0.1 sec to 5 sec. This is in distinct contrast to motions from the mainshock, which are much lower than the predicted motions at periods less than about 1 sec. For distances of 30–60 km the observed motions are lower than the predicted motions, but are still in better agreement with the predictions

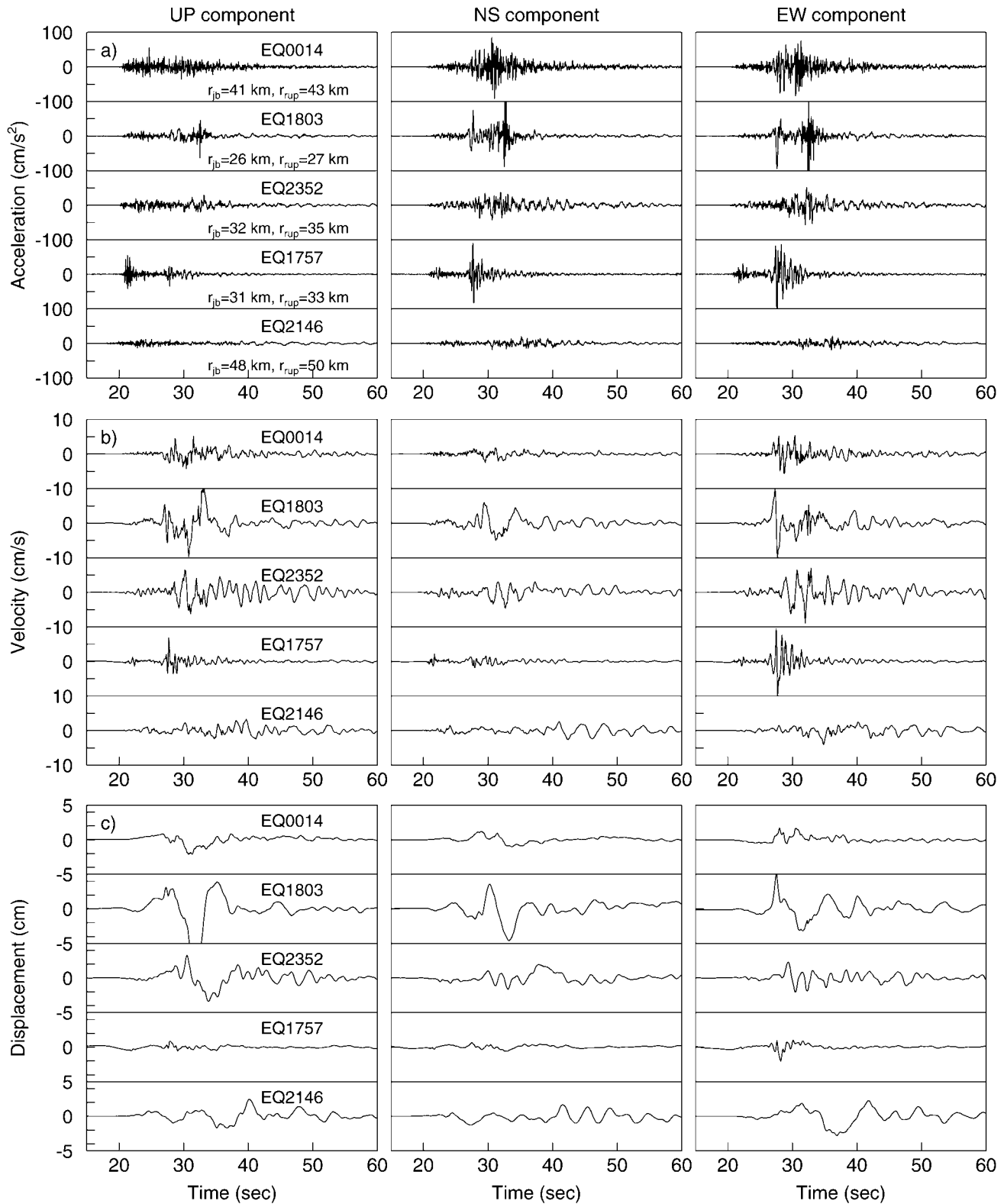


Figure 6. Comparisons of the three-component acceleration, velocity, and displacement time series from the station TCU067 caused by the five events 0014, 1803, 2352, 1757, and 2146. (a) Corrected acceleration time series (see text). (b) Velocity time series obtained by single integration of the corrected accelerations. (c) Displacement time series obtained by double integration of the corrected accelerations. No attempt has been made to align these records except that the records for event 1757 are delayed 10 sec. The exact PGAs and durations of these records are listed in Table 3. The location of the station TCU067 is marked in Figure 1.

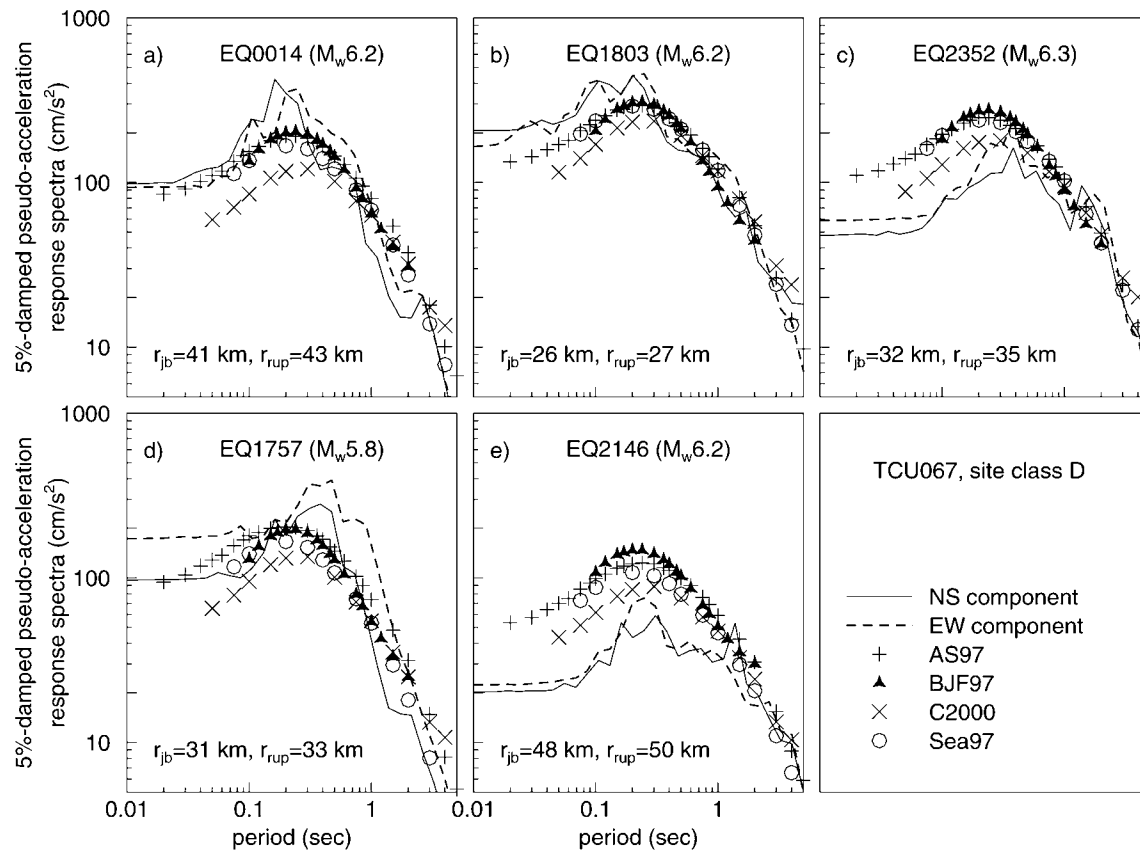


Figure 7. Earthquake- and site-specific comparisons of the observed horizontal response spectra (5% pseudoacceleration response) from the station TCU067 for the five events 0014, 1803, 2352, 1757, and 2146, compared with the predictions from the four equations.

Table 4

Regional Attenuation Coefficients for the Attenuation Function $\log Y = a_1 + a_2 (M - 6) + a_3 \log \sqrt{r_{jb}^2 + h^2}$ to Estimate 5%-Damped Pseudovelocity Response Spectra (cm/sec) of Horizontal Component Developed by Authors Based on *D* Site Records of the Four Reverse-Slip Events 0014, 1803, 2352, and 1757 Using Joyner and Boore's Maxlik Program (Joyner and Boore, 1993).

| Period (sec) | a_1 | a_2 | a_3 | b_5 (BJF97) |
|--------------|-------|-------|--------|---------------|
| 0.10 | 2.440 | 0.453 | -1.468 | -0.934 |
| 0.15 | 2.634 | 0.440 | -1.410 | -0.937 |
| 0.20 | 2.705 | 0.438 | -1.340 | -0.924 |
| 0.30 | 2.678 | 0.446 | -1.207 | -0.893 |
| 0.40 | 2.613 | 0.454 | -1.114 | -0.867 |
| 0.50 | 2.669 | 0.473 | -1.117 | -0.846 |
| 0.75 | 2.577 | 0.565 | -1.056 | -0.813 |
| 1.00 | 2.606 | 0.601 | -1.069 | -0.798 |
| 1.50 | 2.355 | 0.771 | -0.964 | -0.796 |
| 2.00 | 2.119 | 0.857 | -0.862 | -0.812 |
| 2.50 | 1.981 | 0.890 | -0.805 | |
| 3.00 | 1.900 | 0.946 | -0.790 | |
| 4.00 | 1.900 | 1.015 | -0.869 | |
| 5.00 | 1.845 | 1.041 | -0.882 | |

than the motions from the mainshock. The lower motions at greater distance might be due to greater attenuation of motions in the region of Taiwan providing the data used in this article than for the region represented by the mostly California data. We derive regional attenuation equations that show increasing decay with decreasing period.

The comparison of mainshock and aftershock motions with the predicted motions indicates that the low motions for the mainshock are not due to some unusual greater absorption of seismic energy in the central region of Taiwan. It has been recognized before that ground motions from a number of recent large earthquakes whose faulting broke the surface have lower-than-expected high-frequency ground motions. Somerville (2003) pointed out that at short and intermediate periods, the ground motions from earthquakes that produce large surface rupture appear to be systematically weaker than those whose rupture is confined to the subsurface. The observation of different behavior for the mainshock and aftershock motions, whose paths traverse similar geology and for which the recording stations are the same, adds weight to the suggestion that whether a fault breaks to the surface may control the relative excitation of high-frequency energy (the aftershocks did not break to the

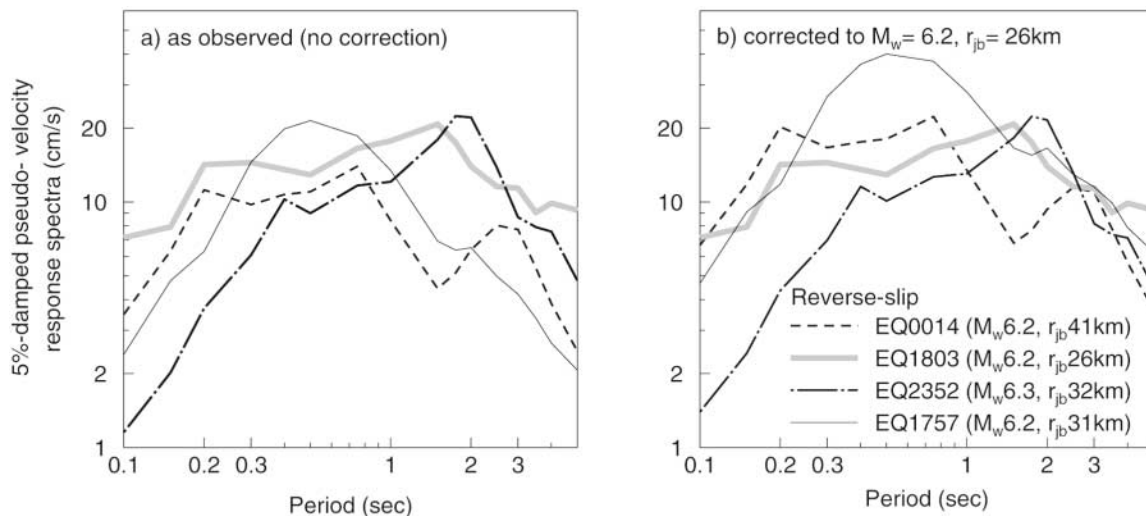


Figure 8. 5%-damped pseudovelocity response spectra for horizontal ground motions at the station TCU067 triggered by the four reverse-slip events 0014, 1803, 2352, and 1757 with and without correction for magnitude and distance dependence. (a) Observed horizontal response spectra without correction, which are the geometric means of the values of the two horizontal components. (b) The response spectra of the three events 0014, 2352, and 1757 have been corrected for geometrical spreading and the magnitude to the distance and magnitude of the record triggered by event 1803, using a regional attenuation function developed by authors based on the records at D sites of the four reverse-slip events using the program maxlik developed by Joyner and Boore (1993) (see text).

surface). Anderson *et al.* (2002) pointed out that earthquakes with high slip rates might produce earthquakes with lower high-frequency energy than earthquakes with lower slip rates. If the aftershocks are on low-slip-rate secondary faults, away from the mainshock rupture surface, this could explain the difference in high-frequency radiation between the mainshock and the aftershocks. Campbell (written comm., 2004) pointed out that nonlinear soil behavior during the ground shaking could contribute the differences between mainshock and aftershock high-frequency ground motions. Of course, other explanations are possible, including the relatively low number of large earthquakes used to derive the ground-motion prediction equations and the effects of earthquake-to-earthquake variability, such that the prediction equations may be controlled at large magnitudes by unusually large motions from one or two events (the databases used by Abrahamson and Silva [1997] and Sadigh *et al.* [1997] do not include any records with magnitude larger than 7.5, and the databases of Boore *et al.* [1997] and Campbell [1997] only include a few records from earthquakes with magnitude larger than 7.5).

The five aftershocks studied here contain a large amount of earthquake-to-earthquake variability in ground motions for a given site. The variations remind us that accurate earthquake-specific predictions of ground motion at a specific site can be difficult. The average ground motions for many earthquakes recorded at a number of stations falling into the same site class can probably be predicted more accurately than

site-specific, earthquake-specific ground shaking. The same conclusion was reached by Boore (2004), based on a review of many observations from other parts of the world.

(E) Observed PHAs and PSAs for oscillator periods between 0.02 sec and 5.0 sec for the five aftershocks and the mainshock used in studying the ratios of observed to predicted motions are available online at the SSA Web site.)

Acknowledgments

We thank Dr. Wu-Cheng Chi and Dr. Doug Dreger for supplying their unpublished article about the source processes of the five aftershocks of the Chi-Chi event. We also thank Dr. Ken Campbell, Dr. Bob Darragh, Dr. Chris Stephens, and Dr. Linda Seekins for their careful corrections and thoughtful suggestions. The Central Weather Bureau of Taiwan and W.H.K. Lee and colleagues for funding, installing, and maintaining the strong-motion network and for making the data from the mainshock and many aftershocks freely available soon after the Chi-Chi earthquake. G.-Q.W. thanks the German Academic Exchange Service (DAAD) for funding through the International Quality Network: Georisks (<http://www.iqn-geo.risk.de>). This research was funded in part by Natural Science Foundation of China Project no. 50178007.

References

- Abrahamson, N. A., and W. J. Silva (1997). Empirical response spectral attenuation relations for shallow crustal earthquakes, *Seism. Res. Lett.* **68**, 94–127.

- Anderson, J. G., J. N. Brune, R. Anooshehpour, and S.-D. Ni (2000). New ground motion data and concepts in seismic hazard analysis, *Curr. Sci.* **79**, 1278–1290.
- Anderson, J. G., J. N. Brune, and S. G. Wesnousky (2002). Physical phenomena controlling high-frequency seismic wave generation in earthquakes, *Proc. 7th National Conference on Earthquake Engineering*, Boston, Massachusetts, 21–25 July 2002.
- Boore, D. M. (1999). Effect of baseline corrections on response spectra for two recordings of the 1999 Chi-Chi, Taiwan, earthquake, *U.S. Geol. Surv. Open-File Rept.* 99-545, 37 pp.
- Boore, D. M. (2001a). Effect of baseline correction on displacement and response spectra for several recordings of the 1999 Chi-Chi, Taiwan, earthquake, *Bull. Seism. Soc. Am.* **91**, 1199–1211.
- Boore, D. M. (2001b). Comparisons of ground motions from the 1999 Chi-Chi earthquake with empirical predictions largely based on data from California, *Bull. Seism. Soc. Am.* **91**, 1212–1217.
- Boore, D. M. (2004). Can Site Response be Predicted? *J. Earthquake Eng.* **8**, no. 1, 1–41.
- Boore, D. M., W. B. Joyner, and T. E. Fumal (1997). Equations for estimating horizontal response spectra and peak acceleration from western north american earthquakes: a summary of recent work, *Seism. Res. Lett.* **68**, 128–153.
- Building Seismic Safety Council (1998). 1997 Edition NEHRP recommended provisions for seismic regulations for new buildings, FEMA 302/303, developed for the Federal Emergency Management Agency, Washington, D.C.
- Campbell, K. W. (1997). Empirical near-source attenuation relationships for horizontal and vertical components of peak ground acceleration, peak ground velocity, and pseudo-absolute acceleration response spectra, *Seism. Res. Lett.* **68**, 154–179.
- Campbell, K. W. (2000). Erratum to Empirical near-source attenuation relationships for horizontal and vertical components of peak ground acceleration, peak ground velocity, and pseudo-absolute acceleration response spectra by Kenneth W. Campbell, *Seism. Res. Lett.* **71**, 353–355.
- Campbell, K. W. (2001). Strong motion attenuation relations: commentary and discussion of selected relations (appendix), in *IASPEI Handbook of Earthquake and Engineering Seismology*, W. H. K. Lee (Editor), Academic Press, San Diego.
- Campbell, K. W., and Y. Bozorgnia (2003). Updated near-source ground-motion (attenuation) relations for the horizontal and vertical components of peak ground acceleration and acceleration response spectra, *Bull. Seism. Soc. Am.* **93**, 314–331.
- Chi, W.-C., and D. Dreger (2004). Crustal deformation in Taiwan: results from finite source inversions of six $M_w > 5.8$ Chi-Chi aftershocks, *J. Geophys. Res.* **109**, B07305, doi:10.1029/2003JB002606.
- Ellsworth, W. L., M. Çelebi, J. R. Evans, E. G. Jensen, D. J. Nyman, and P. Spudich (2004). Processing and modeling of the Pump Station 10 record from the November 3, 2002, Denali fault, Alaska earthquake, *Proc. 11th International Conference on Soil Dynamics and Earthquake Engineering*, Berkeley, California, 7–9 January 2004.
- Joyner, W. B., and D. M. Boore (1993). Methods for regression analysis of strong-motion data, *Bull. Seism. Soc. Am.* **83**, 469–487.
- Lee, C. T., C. T. Cheng, C. W. Liao, and Y. B. Tsai (2001a). Site classification of Taiwan free-field strong-motion stations, *Bull. Seism. Soc. Am.* **91**, 1283–1297.
- Lee, W. H. K., T. C. Shin, and C. F. Wu (2001b). CWB free-field strong-motion data from three major aftershocks of the 1999 Chi-Chi earthquake: processed acceleration data files on CD-ROM, CWB Strong-Motion Data Series CD-002, Seismological Observation Center, Central Weather Bureau, Taipei, Taiwan, 28 August 2001.
- Lee, W. H. K., T. C. Shin, and C. F. Wu (2001c). CWB free-field strong-motion data from 30 early aftershocks of the 1999 Chi-Chi earthquake: processed acceleration data files on CD-ROM, CWB Strong-Motion Data Series CD-003, Seismological Observation Center, Central Weather Bureau, Taipei, Taiwan, 31 August 2001.
- Sadigh, K., C.-Y. Chang, J. A. Egan, F. Makdisi, and R. R. Youngs (1997). Attenuation relationships for shallow crustal earthquakes based on California strong motion data, *Seism. Res. Lett.* **68**, 180–189.
- Somerville, P. G. (2000). Magnitude scaling of near fault ground motions, *EOS, Trans. Am. Geophys. Union* **81** (fall meeting suppl.), available at <http://www.agu.org/meeting/waisfm00.html>.
- Somerville, P. G. (2003). Magnitude scaling of the near fault rupture directivity pulse, *Phys. Earth Planet. Interiors* **137**, 201–212.
- Wells, D. L., and K. J. Coppersmith (1994). New empirical relationships among magnitude, rupture length, rupture width, rupture area, and surface displacement, *Bull. Seism. Soc. Am.* **84**, 974–1002.
- Wang, G.-Q. (2001). The characteristics of near-fault ground motion caused by the 1999, Chi-Chi, Taiwan earthquake, *Ph.D. Thesis*, Institute of Geology, China Seismological Bureau (in Chinese).
- Wang, G.-Q., D. M. Boore, H. Igel, and X.-Y. Zhou (2003). Some Observations on collocated and closely spaced strong ground-motion records of the 1999 Chi-Chi, Taiwan, earthquake, *Bull. Seism. Soc. Am.* **93**, 674–693.
- Wang, G.-Q., X.-Y. Zhou, Z.-J. Ma, and P.-Z. Zhang (2001). Data files from “A preliminary study on the randomness of response spectra of the 1999 Chi-Chi, Taiwan, earthquake,” *Bull. Seism. Soc. Am.* **91**, 1388–1389.
- Wang, G.-Q., X.-Y. Zhou, P.-Z. Zhang, and H. Igel (2002). Characteristics of amplitude and duration for near fault strong ground motion from the 1999 Chi-Chi, Taiwan, earthquake, *Soil Dyn. Earthquake, Eng.* **22**, 73–96.

Department of Earth and Environmental Sciences
University of Munich
Munich, 80333 Germany
gwang@ncat.edu
igel@geophysik.uni-muenchen.de
(G.-Q.W., H.I.)

U.S. Geological Survey, MS 977
345 Middlefield Road
Menlo Park, California 94025
boore@usgs.gov
(D.M.B.)

College of Architectural and Civil Engineering
Beijing University of Technology
Beijing, 100022 People's Republic of China
zhouxy@bjpu.edu.cn
(X.-Y.Z., G.-Q.W.)

Manuscript received 17 November 2003.